



Article

# Application of Resistometric Sensors for Real-Time Corrosion Monitoring of Coated Materials

Kateryna Popova <sup>1,\*</sup>, Maria Fátima Montemor <sup>2</sup> and Tomáš Prošek <sup>1,\*</sup>

<sup>1</sup> Department of Metallic Construction Materials, University of Chemistry and Technology Prague, Technopark Kralupy, Nám. G. Karse 7, 278 01 Kralupy nad Vltavou, Czech Republic

<sup>2</sup> Centro de Química Estrutural, Institute of Molecular Sciences, Departamento de Engenharia Química, Instituto Superior Técnico, Universidade de Lisboa, Av. Rovisco Pais, 1049-001 Lisbon, Portugal; mfmontemor@tecnico.ulisboa.pt

\* Correspondence: kateryna1.popova@vscht.cz (K.P.); tomas.prosek@vscht.cz (T.P.); Tel.: +420-220-446-125 (K.P.)

**Abstract:** Highly sensitive resistometric sensors were applied for the real-time corrosion monitoring of carbon steel protected with a polyolefin coating with and without an inhibitor under static and dynamic atmospheric and immersion conditions. The results were compared with conventional electrochemical impedance spectroscopy (EIS) data. An increase in the coating thickness from 20 µm to 50 µm and an addition of 1wt.% tannic acid significantly improved the coating corrosion stability. Based on the real-time corrosion data, the drying stage of atmospheric exposure in a chloride-rich environment was found to be the most critical. The highest corrosion rate was detected at 50% relative humidity when the electrolyte corrosiveness in coating defects reached the maximum. Resistometric sensors have the potential to become an interesting alternative for evaluating coating performance and degradation mechanisms in both laboratory and industrial applications.

**Keywords:** organic coatings; real-time corrosion monitoring; resistometric technique; electrochemical impedance spectroscopy; carbon steel



**Citation:** Popova, K.; Montemor, M.F.; Prošek, T. Application of Resistometric Sensors for Real-Time Corrosion Monitoring of Coated Materials. *Corros. Mater. Degrad.* **2024**, *5*, 573–592. <https://doi.org/10.3390/cmd5040026>

Academic Editor: Wolfram Fürbeth

Received: 27 September 2024

Revised: 27 October 2024

Accepted: 15 November 2024

Published: 19 November 2024



**Copyright:** © 2024 by the authors. Licensee MDPI, Basel, Switzerland. This article is an open access article distributed under the terms and conditions of the Creative Commons Attribution (CC BY) license (<https://creativecommons.org/licenses/by/4.0/>).

## 1. Introduction

The corrosion of metallic materials has huge economic, environmental and cultural impacts. The financial losses associated with corrosion damage are estimated to be around 3–4% of global gross domestic product (GDP) [1–3]. In addition to the economic costs and technological delays, corrosion can lead to sudden industrial and transport failures that may cause environmental catastrophes and hazards that endanger health and lives [3–5]. Approaches to the effective corrosion prevention and management can be divided into several broad categories including the alteration of the environment by changing some of its physical or chemical properties, the selection of the material resistant to corrosion under the given conditions, the proper design of the metallic structures, electrochemical corrosion protection and the application of protective coatings [6]. Among these, the application of organic coatings is the most used way to protect metallic structures from the corrosive environment [7,8]. They provide a barrier layer that physically separates the bare metal from corrosive environments [7,9,10]. Even very good coating systems contain inhomogeneities such as pores, pinholes, cracks, air bubbles and other defects that create preferential pathways for the uptake of moisture, oxygen and corrosive species [3,9,11]. Over time, these species can reach the bare metal and initiate corrosion [9]. Therefore, in addition to the barrier effect, the coating must be able to inhibit the corrosion process when the physical barrier is disrupted, thereby increasing its protectiveness and service life [7,11,12]. This can be achieved by adding corrosion inhibition pigments into the coating system [3,7]. The protective mechanisms of the most common corrosion inhibitors include the passivation of the substrate, formation of a protective layer of insoluble metal complexes,

blocking of active corrosion sites, physical hindrance of the electrolyte diffusion pathways or formation of complexes with corrosive species, such as chloride ions [3,10,12]. Sacrificial protection is achieved by the preferential corrosion of a more electrochemically active metal present in the coating system in the form of pigment or flakes in electrical contact with the substrate [3]. The general requirements for effective anti-corrosion coatings include the combination of properties such as a good barrier effect, the presence of an additive that inhibits the corrosion process, good adhesion to the substrate, and compatibility with additional layers such as topcoats [7]. The other specific requirements depend on the operating environment and the duration of exposure [3].

The service conditions to which the coated materials may be exposed can be divided into three main categories: immersion (including exposure to fresh water, sea water, soil and specific electrolytes), splash zone and atmosphere [3]. The corrosivity of the environments to which the coated structures may be exposed is classified in the standard ISO 12944-2 [13]. Unlike the first group, which is characterized by relatively stable conditions, atmospheric and splash zone exposures involve locally alternating conditions of wetting and drying, heating, precipitation, condensation and UV irradiation. Of these, wetting and drying cycles (night/morning condensation, daytime drying) and prolonged condensation are known to be particularly corrosive [14,15]. Atmospheric corrosivity can vary significantly depending on climate, pollution levels and distance from the sea [3]. For example, industrial environments are characterized by high contents of solid particles, increased levels of sulphur dioxide and acid rain, while marine atmospheres are characterized by the high deposition of chloride ions [3]. Therefore, the corrosive environmental effects can vary significantly, and different environments must be considered separately in terms of their corrosiveness towards the coated structures.

Approaches to evaluating the protective effectiveness of coatings can be divided into three main groups: (i) the evaluation of the corrosion performance of coated structures in service; (ii) standard accelerated corrosion testing; and (iii) conventional and advanced laboratory analysis [11].

The corrosion performance evaluation of industrial coating systems in service is usually realized by visual inspection. It requires considerable manpower, may induce a safety risk, and is often required on structures that are difficult to assess. In addition, the results of the inspection are subjective and depend on the skill and experience of the inspector, and corrosion processes initiated under the coating may be overlooked [16]. Among alternative non-destructive techniques, ultrasonic inspection is the most widely used [17]. It is sensitive and accurate but requires extensive knowledge to operate the instrument and the presence of the operator on the site [17]. Both described approaches are periodic inspections, which means that the degradation of the structure may occur between inspection events [16].

Accelerated corrosion tests include the traditional neutral salt spray test (NSST), in which 5% sodium chloride solution is sprayed on samples at an elevated temperature, and cyclic tests, which consist of alternating phases of electrolyte application, drying and wetting, and eventually also UV irradiation and temperature gradients [3,11,18]. Sample preparation and the evaluation of results usually follow the standard procedures defined in regulations, e.g., the EN ISO 4628 series standards [19].

Conventional electrochemical techniques are used to evaluate the performance and durability of anti-corrosion coatings in the laboratory [3]. These techniques are based on the electrochemical nature of the corrosion process and evaluate the electrical properties of the metal/coating/solution system [3,20]. Their advantage is their ability to provide information on coating degradation before it can be visually observed [3,11]. The most widely used electrochemical impedance spectroscopy (EIS) method was first applied to study anti-corrosion coatings by Takenouti et al. in 1972 [11]. EIS is a non-destructive technique applied for the evaluation of the barrier and protective properties of coatings, the effectiveness of corrosion inhibitors, water uptake, the presence of defects, interface reactivity and coating adhesion [11,12,14,21,22]. A low-amplitude AC voltage is applied at an open

circuit potential or at a potential of choice, and the AC response recorded as impedance spectra at a range of frequencies using a conventional three-electrode electrochemical cell. The working electrode is a sample under investigation, the reference one can be, e.g., a saturated calomel electrode (SCE), and the counter electrode is made of an inert material such as a platinum wire or a carbon rod [14,23,24]. Impedance data are usually presented as Nyquist and Bode plots [23,25]. The interpretation of the data is based on equivalent electrical circuits combining resistors and capacitors, and some specific elements include the constant phase element (CPE) and Warburg impedance, which represent electrochemical processes taking place in the system [11,14,24,26]. Consequently, changes in the values of the individual components indicate the behaviour and performance of a coating system [3]. EIS is a powerful tool due to its high sensitivity and ability to provide a complete view of the mechanisms and kinetics of coating degradation and metal corrosion [27,28]. Still, it has several limitations, including complex data interpretation, which requires experience and detailed knowledge of the system under investigation [26]. Also, the application of EIS data to predict coating lifetime remains a challenge [3]. Amirudin and Thierry [26] and Margarit-Mattos [27], thus, pointed out the need to use independent complementary techniques for the validation and correct interpretation of EIS data.

To study local processes occurring around defects, inhibiting and self-healing mechanisms, advanced spatially resolved electrochemical tools are used [7]. These include scanning electrochemical microscopy (SECM) [11,20], the scanning vibrating electrode technique (SVET) [11,12,20], the scanning ion selective electrode technique (SIET) [12,20], localized electrochemical impedance spectroscopy (LEIS) [11,20] and the scanning Kelvin probe (SKP) [3,11,20,22].

The described laboratory techniques provide valuable information on the coating protection efficiency and degradation mechanisms. However, a significant gap exists between the evaluation of coating performance under real operating conditions, accelerated corrosion tests and laboratory studies. This is largely due to the fact that the laboratory techniques, with the exception of SKP, require the presence of a conductive electrolyte to establish an electrical connection between the electrodes [4,11]. As a result, the measurements are usually performed in immersion, and their application in dynamic atmospheric conditions is limited [4,29]. EIS has, thus, been adapted for atmospheric corrosion studies, as shown in a review by Xia et al. [28]. For field monitoring, the measurement is usually performed at one or two frequencies instead of scanning a wide range of frequencies to simplify the instrumentation, shorten the measurement time and allow the fast screening of a large number of samples and painted structures [28,30]. An electrical connection between electrodes is achieved by using an external electrolyte, such as a conductive gel, a wet cloth, or a soaked filter paper. The disadvantage of this approach is that the choice of the measurement frequency can affect the result, while the introduction of an external electrolyte changes the environment and accelerates corrosion [28]. Consequently, there is a need to develop a system for the real-time evaluation of coating performance that can be used in atmospheric accelerated corrosion tests simulating the real operating conditions or directly implemented in service [29].

Several attempts have been made to adapt the existing techniques of atmospheric corrosion monitoring for the evaluation of coating systems. Deng et al. measured the corrosion rate of steel under polymeric and Al-Zn coatings using fiber-optic corrosion sensors embedded under the coatings [17]. They used fiber Bragg grating sensors, which reflect a specific wavelength of incoming light that meets the Bragg conditions and transmit all the others. The Bragg wavelength is defined by the refractive index of the fiber and a grating pitch, and its shift can be caused by temperature variations or external tension. The formation of voluminous corrosion products on the metallic surface under the coating causes an increase in strain and a change in the detected wavelength, from which the corrosion rate can be calculated. The authors performed the experiment via immersion in a 3.5% NaCl solution, but the measurement can, in principle, be conducted in atmospheric conditions [4]. Alamin et al. [31,32] and Sunny et al. [33] investigated the corrosion of coated

steel using the low-frequency radio frequency identification (LF RFID) technique. Their setup consisted of a reader and a tag, the former activating the latter with an electromagnetic signal and reading the signal transmitted back. When the tag is placed near a metallic structure, its resonant frequency is shifted. An eddy current is generated, creating a secondary magnetic field that is opposite to the primary one generated by the reader. Since the electromagnetic properties (conductivity and permeability) of the material vary as corrosion products form on the surface, the corrosion's extent can be determined by measuring these properties. Using this principle, the authors tested six coated and uncoated steel panels after different periods of atmospheric exposure and obtained a relative order of their corrosion degradation [31–33]. Daneshian et al. used CorRES carbon steel sensors coated with 300  $\mu\text{m}$  epoxy coatings with a scribe to measure the free corrosion current using the linear polarization resistance (LPR) technique together with environmental parameters at an outdoor coastal corrosion station in Norway for one year and analyzed the effect of the particular climatic parameters on the corrosion response [34]. The data were then used as an input to predict atmospheric corrosion of marine structures using a time series machine learning framework [35]. However, only corrosion in the scribe was measured, and the coating performance was not evaluated in the study. Recently, Tatsuoka presented a coated atmospheric corrosion monitor (ACM) [36]. The sensor consisted of two different metal electrodes, one acting as a cathode and the other as an anode [4]. At high relative humidity (RH), a thin layer of electrolyte formed on the surface, providing an electrical connection between the electrodes, and a galvanic current was generated. The value of the galvanic current has been reported to have a good correlation with the corrosion rate of the anodic metal [4].

The described methods provide only an indirect assessment of the corrosion response of a coated metal. Furthermore, only ACM and CorRES sensors are commercially available, while the application of fiber-optic and RFID sensors remains at the calibration and laboratory testing stage and is limited to model materials [29].

The resistometric technique of real-time atmospheric corrosion monitoring is an interesting alternative to the described approaches. The technique has been successfully used for the atmospheric corrosion monitoring of carbon steel, zinc, aluminium, copper and lead in laboratory studies [37–43], accelerated corrosion tests [29,44–48], cultural heritage institutions [49–53], vehicles [54,55] and the monitoring of corrosion under thermal insulation [56]. The measurement is based on recording the electrical resistance of a thin metal track applied on a non-conductive substrate and exposed to a corrosive environment. Electrical resistance  $R$  depends on the resistivity  $\rho$  characteristic for the given material and the geometric parameters of the track (thickness  $t$ , length  $l$  and width  $w$ ) [29]:

$$R = \rho \frac{l}{w \times t} \quad (1)$$

For a metal track of given resistivity and length, the evolution of electrical resistance over time directly reflects the cross-sectional loss of the material caused by corrosion and can, therefore, be easily interpreted in terms of the actual corrosion rate. As the technique is not electrochemical in nature, no electrolyte is required and the measurement can be carried out continuously even in a dry atmosphere.

Together with the geometrical parameters of the track, the electrical resistance depends on the temperature according to Equation [57]:

$$R_T = (1 + \alpha \Delta T) R_{init}, \quad (2)$$

where  $R_T$  is the resistance of the metal track at a given temperature  $T$ ,  $R_{init}$  is its initial resistance,  $\Delta T$  is the difference between the initial and given temperatures and  $\alpha$  is the temperature coefficient of the material. To eliminate the temperature effect on the electrical resistance, one part of the sensor (sensing track) is exposed to the corrosive environment and its resistance is affected by both temperature variations and material loss caused by

corrosion, while another (reference) track is protected during exposure, and its resistance changes only due to temperature variations.

The actual corrosion depth ( $CD$ ) of the actively corroding sensing track can then be calculated according to Equation (3):

$$CD = t_{init} \left( \frac{R_{ref,init}}{R_{sens,init}} - \frac{R_{ref}}{R_{sens}} \right), \quad (3)$$

where  $t_{init}$  is the initial thickness of the metal track,  $R_{ref,init}$  and  $R_{sens,init}$  are the initial reference and sensing track resistances, and  $R_{ref}$  and  $R_{sens}$  are the actual reference and sensing track resistances [29,44,56]. The actual corrosion rate ( $CR$ ) of the sensing track can be calculated as a derivative of  $CD$  over time.

The main advantage of the resistometric method is the ability to monitor the corrosive effect of the environment on the exposed sample in real time with a continuous and quantitative assessment of the corrosion rate [37]. Sensors can be manufactured from a wide range of pure metals and alloys, including bare and stainless steel, zinc, aluminium, copper, silver and lead. The sensitivity of the sensor increases with decreasing thickness, while the greater thickness ensures its longer lifetime. Therefore, depending on the environmental corrosiveness, a compromise between sensor lifetime and sensitivity can be achieved by selecting an optimal sensor thickness.

Resistometric sensors have so far been used mainly for monitoring bare metal surfaces, but a few attempts have also been made to use them to monitor coated materials. In contrast to the electrochemical methods described above, the technique does not evaluate the deterioration of the coating but the resulting corrosion of the metal substrate [16], which is the parameter of interest for engineers and asset owners [16].

Diler et al. [29] exposed zinc galvanized and organic coated steel sensors with and without surface defects in the Volvo STD423-0014 accelerated corrosion test to study the corrosion kinetics and compare the results with bare steel and zinc. For the organic coated sensors with a model defect, the effect of the defect geometry on the sensor response was observed and had to be recalculated and compensated for. For a coated sensor without artificial defects, the measurement allowed for the accurate determination of the onset of substrate corrosion, i.e., the coating failure. The authors concluded that the technique has the potential to be used in practice and reduce the number of visual inspections in the field and during accelerated corrosion tests [29]. Zajec et al. [14,16] used resistometric and EIS sensors to monitor the corrosion of carbon steel under coatings of different thicknesses in a salt spray test and in chambers with increased humidity and  $SO_2$  supply. The authors reported a high sensitivity of EIS for detecting coating degradation at very early stages, whereas the resistometric probes could only detect the initiation and propagation of the underlying metal corrosion. On the other hand, the authors considered that the thickness reduction obtained from the resistometric sensors was, in principle, more reliable for assessing substrate corrosion under the coating, since the measured electrical resistance was in a simple relationship with the corrosion depth and no additional modeling was required. In addition, the resistometric sensors did not require immersion in the electrolyte, thus avoiding the ambiguities of electrolyte chemistry and immersion time. They therefore recommended using the resistometric sensors for field applications rather than the EIS probes. Švadlena and Stoulil [37] used copper and carbon steel sensors to compare two acrylate copolymers in terms of their ability to protect historic metallic materials. They sensitized the steel sensor surface by contaminating it with a chloride solution before applying the coating and calculated the diffusion coefficient of water in the coating from the time at which water molecules penetrated the coating and caused the corrosion rate to increase. Copper sensors were used to compare the coatings' protective properties against specific air pollutants at elevated humidity.

The aim of the present study was to apply a state-of-the-art wireless real-time corrosion monitoring system for testing the performance of an organic coating under static and dynamic atmospheric conditions and in immersion, as well as to compare the results with

the conventional EIS technique. This study demonstrates the applicability of resistometric sensors under three different types of environmental conditions, provides a correlation between climatic data and the coating performance in the real time and assesses the advantages and potential critical points of using resistometric sensors for the monitoring of corrosion under organic coatings. A polyolefin coating was selected for this study because of its previously reported good mechanical properties, low oxygen permeability, good adhesion to steel and high efficiency against electrolyte uptake when immersed in a chloride solution [58,59]. The coating was also modified with an inhibitor to obtain coatings with identical thicknesses and different protective abilities [21,58,59].

## 2. Materials and Methods

### 2.1. Resistometric Sensors and Monitoring System

The experiments were carried out using the CorrSen monitoring system (produced by Gema Ltd., Unhošť, Czech Republic), which consists of wireless loggers with resistometric sensors, data collectors, and an online interface for data evaluation and presentation. Sensitive carbon steel sensors with initial thicknesses of 25  $\mu\text{m}$  were used. Carbon steel was chosen for the current study as the most widely used structural material. The sensor consists of four metal tracks, one reference and three sensing, as shown in Figure 1. By using three sensing tracks simultaneously, the reproducibility of the measurement was increased.

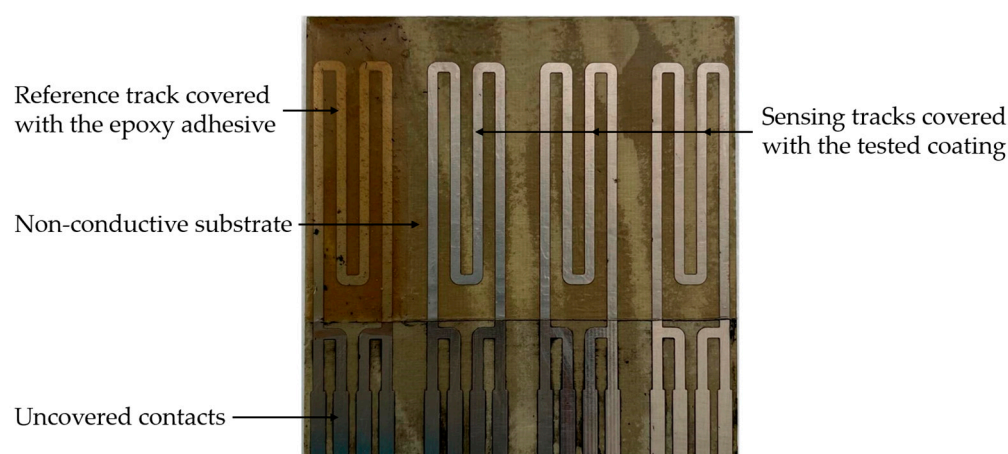


**Figure 1.** Coated resistometric sensor Fe—25  $\mu\text{m}$ .

First, the contacts of the sensor were temporarily masked with tape. The reference track was covered with Araldite Rapid two-component epoxy adhesive (Huntsman Advanced Materials, Basel, Switzerland) to protect it from corrosion. Then, the coating was applied to the three measuring tracks following the procedure described in the following section. Once the coating had cured, the tape was removed from the contacts. Sensors prepared for atmospheric tests were inserted into loggers and the contacts were sealed with epoxy adhesive to prevent corrosion. Sensors for immersion exposures were soldered to 2 m long cables, and the connections were covered with epoxy adhesive.

### 2.2. Coating Preparation

The commercial aqueous acid modified polyolefin dispersion CANVERA™ 1110 (produced by Dow Chemicals, Midland, MI, USA) was used as the protective coating in this study. The coating was applied to the sensing tracks to achieve two dry coating thicknesses of 20 and 50  $\mu\text{m}$ . Dip and bar coating processes reported in the literature were tested [21,58,59]. The obtained coatings were heterogeneous and the reproducibility was poor, probably due to the complex surface of the sensor (combination of metallic tracks and polymer substrate). Therefore, a different coating preparation method was proposed. First, the liquid dispersion was mixed with ethanol at a 2:1 mass ratio and homogenized

using a magnetic stirrer in order to dilute the dispersion for easier application. Then, the amount of the dispersion–ethanol mixture  $V_{mixture,wet}$  that needed to be applied to obtain the required thickness of the dry coating  $t_{coating,dry}$  was calculated based on the knowledge of the sensor area, the density of the mixture and dry coating and the mass reduction in the coating during drying. The density of the mixture  $\rho_{mixture,wet}$  and cured coating  $\rho_{coating,dry}$  were measured to be  $1.06 \text{ g cm}^{-3}$  and  $0.97 \text{ g cm}^{-3}$ , respectively. The mass reduction  $\Delta m$  in the mixture after curing was 0.645 of the initial weight. The area to be covered with the coating  $S$  was measured for each sensor individually. The volume of the dispersion–ethanol mixture required to achieve the final dry coating thickness was then calculated according to Equation (4).

$$V_{mixture,wet} = \frac{1.5 \cdot S \cdot t_{coating,dry} \cdot \rho_{coating,dry}}{(1 - \Delta m) \cdot \rho_{mixture,wet}} \quad (4)$$

Index 1.5 sources from the dilution ratio of the dispersion–ethanol mixture.

The calculated volume of the wet mixture to be applied on the sensor was divided by 2 or 3 for a final coating thickness of 20 or 50  $\mu\text{m}$ , respectively. The surfaces of the sensors were cleaned with ethanol prior to coating application. The calculated portion of the mixture was applied to the sensor surface using a micropipette and evenly distributed over the surface. The sensor was then placed in an oven at  $175 \text{ }^\circ\text{C}$  for 15 min, then the oven was switched off and the sensor was allowed to cool slowly to avoid cracking. Polyolefin melted at  $160 \text{ }^\circ\text{C}$ , which helped the curing process through cross-linking. At  $175 \text{ }^\circ\text{C}$ , the white suspension became completely transparent and formed strong contact with the substrate [58]. The remaining amount of the mixture was then applied to the surface in one or two parts and the curing process was repeated. This procedure led to formation of a more homogeneous coating layer, avoiding bubble formation during solvent evaporation.

In addition to the pure polyolefin dispersion, a coating with an inhibitor was tested. Tannic acid was chosen as a non-toxic, environmentally friendly polyphenolic inhibitor, which formed complexes with the metallic substrate, creating an additional anti-corrosive thin film on the surface [9,60]. The dry tannic acid powder (produced by Sigma Aldrich, Saint Louis, MO, USA) was preconditioned in an oven at  $50 \text{ }^\circ\text{C}$  for 2 h and then added to the dispersion–ethanol mixture at an amount of 1 wt.% with respect to the wet polyolefin dispersion (i.e., 0.66 wt.% of the wet dispersion–ethanol mixture). The modified dispersion was applied to the sensors using the procedure described above at a 20  $\mu\text{m}$  dry thickness.

The resulting coating thickness was verified after curing using the Leica DMS 300 (Leica, Wetzlar, Germany) optical microscope on the cross-section. The final thicknesses of the coatings were  $54 \pm 5 \mu\text{m}$  and  $21 \pm 3 \mu\text{m}$ , respectively.

Along with the coated sensors, a bare sensor was exposed in each test for comparison.

### 2.3. Accelerated Corrosion Tests

Three accelerated corrosion tests were carried out to evaluate the protective abilities of the coatings under both atmospheric and immersion conditions. In all tests, the electrical resistance of the sensors was measured with the CorrSen loggers at a 2 min interval. During the atmospheric tests, the temperature and RH were recorded by the loggers simultaneously. All the tests were conducted at a laboratory temperature of  $24 \pm 3 \text{ }^\circ\text{C}$ . The maximum exposure duration was 2 months. If a sensor corroded completely, the measurement was terminated earlier.

The static atmospheric corrosion test was carried out at constant condensation to simulate the conditions of standard tests for the evaluation of coating resistance to humid atmospheres and to compare it with results of cyclic exposures described below. The sensors with loggers were placed in a plastic box together with beakers filled with demineralized water, as shown in Figure 2. The box was then hermetically sealed. The RH inside the box showed a gradual increase to 99–100%.

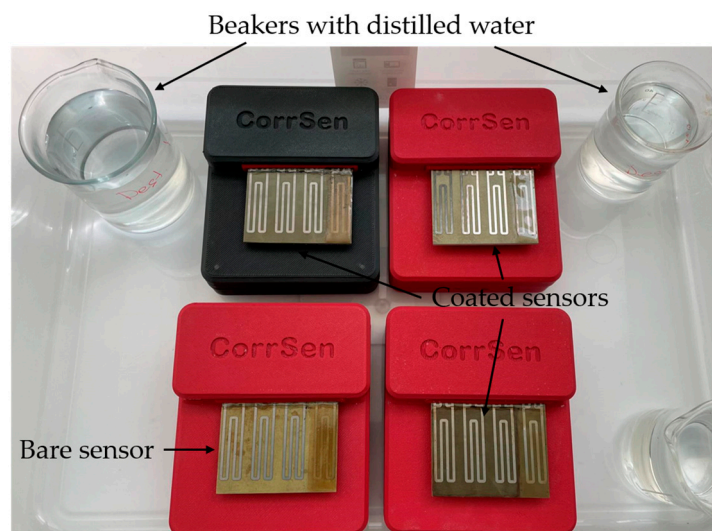


**Figure 2.** Sensors during the static atmospheric test.

In the cyclic atmospheric corrosion test, the sensors were subjected to alternating phases of chloride deposition, wetting and drying. The test was designed to allow the sensors to experience dynamic humidity transitions, and it could be carried out manually during working days without any need for special equipment. The weekly cycle of the test is shown schematically in Figure 3.

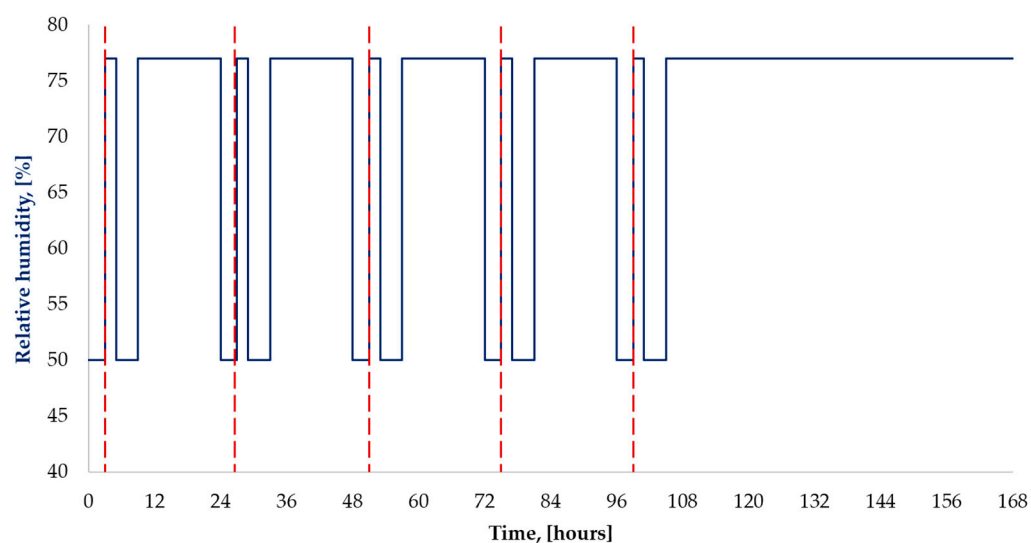


**Figure 3.** The one-week cycle of the cyclic atmospheric corrosion test; red dashed lines indicate NaCl deposition.

At the beginning of each daily cycle, the sensors were left in the laboratory for two hours to simulate the dry phase. The RH measured in the laboratory during the two months was  $53\% \pm 11\%$ . Then, a 0.05 M (0.3 wt.%) NaCl solution at the natural pH was applied to the sensors by spraying, and the loggers were placed for 2 h in a box with beakers filled with saturated  $\text{KNO}_3$  solution (Figure 4) to keep the RH at 77%. This phase was considered the wet phase, since the RH was kept above the deliquescence RH for NaCl of 75% [44,61]. Wetting was also confirmed visually, as the sensor surface was covered with electrolyte droplets. After 2 h, the sensors were removed from the box and left in the laboratory for another 3 h, simulating the second dry phase. Finally, the sensors were returned to the box and left in the wet atmosphere overnight (16 h). The wet phase continued over the weekends.



**Figure 4.** The sensors during the cyclic atmospheric test; the beginning of the wet phase after spraying with NaCl solution.

A short verification test was carried out to confirm the observations from the cyclic atmospheric test and to evaluate the effect of the chloride concentration. Two sensors with 50  $\mu\text{m}$  coatings without the inhibitor were exposed to the same climatic cycle. One sensor was sprayed with 1.5 wt.% NaCl solution, i.e., 5-fold more concentrated, while the second sensor was sprayed with demineralized water.

The immersion test was introduced to compare the coating performance in atmospheric and immersion conditions and to compare results obtained by the resistometric and EIS techniques. The sensors on the cables were placed in beakers with 0.3 wt.% NaCl solution, as illustrated in Figure 5. The amount of the solution was adjusted to ensure that the sensing parts of the sensors were submerged, while the contacts were above the solution level to avoid extensive corrosion. Demineralized water was periodically added to the beakers to keep the volume of the solution constant.

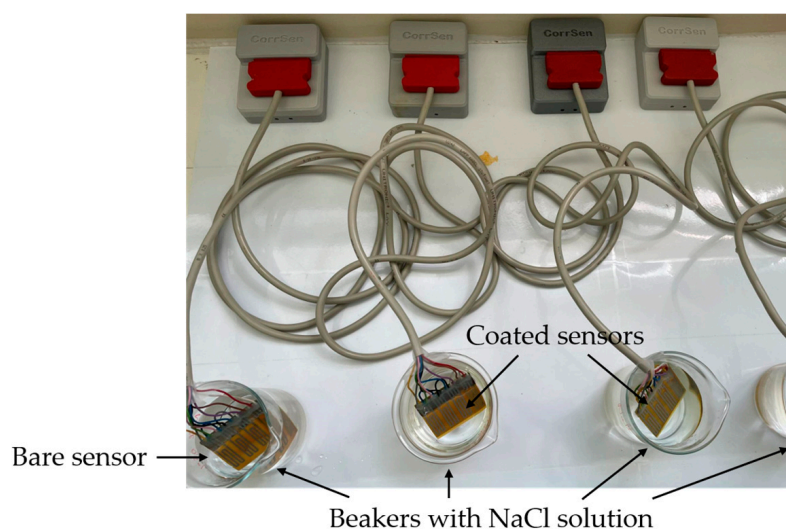


**Figure 5.** The sensors exposed in the immersion test.

#### 2.4. Electrochemical Impedance Spectroscopy

Electrochemical impedance spectroscopy (EIS) was used as a conventional technique to compare and validate the resistometric measurements. A Gamry Reference REF 600 potentiostat (Gamry Instruments, Warminster, PA, USA) was used in the conventional

three-electrode cell configuration inside a Faraday cage (Figure 6). A saturated calomel electrode (SCE; model HI5412, Hanna Instruments, Woonsocket, RI, USA) was used as the reference electrode, a platinum coil as the counter electrode, and the coated sensor as the working electrode. The contacts of the sensor’s sensing tracks were electrically connected with conductive adhesive prior to the experiment to measure the impedance across all three sensing tracks, with a total area of 3.36 cm<sup>2</sup>. The electrodes were immersed in a 0.3 wt.% NaCl solution. Demineralized water was periodically added to the beaker to maintain a constant volume of the solution. Impedance spectra were collected at open circuit potential under a 10 mV (rms) sinusoidal perturbation in a frequency range from 100 kHz to 50 mHz. The EIS measurements were performed on the 50 μm-coated sensor and the bare sensor. The 50 μm coating was chosen to demonstrate the sensitivity of the technique on the coating system with the best expected protective ability.

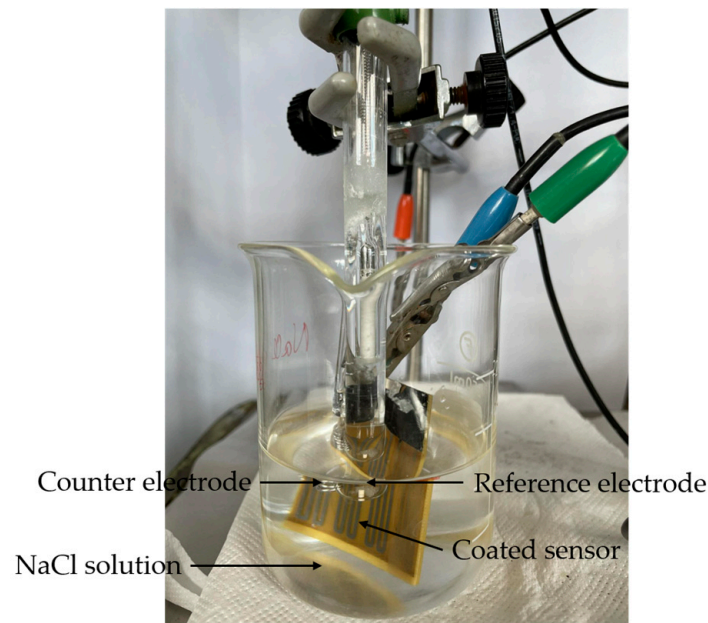


Figure 6. EIS measurement.

The experimental work is summarized in the flowchart shown in Figure 7.

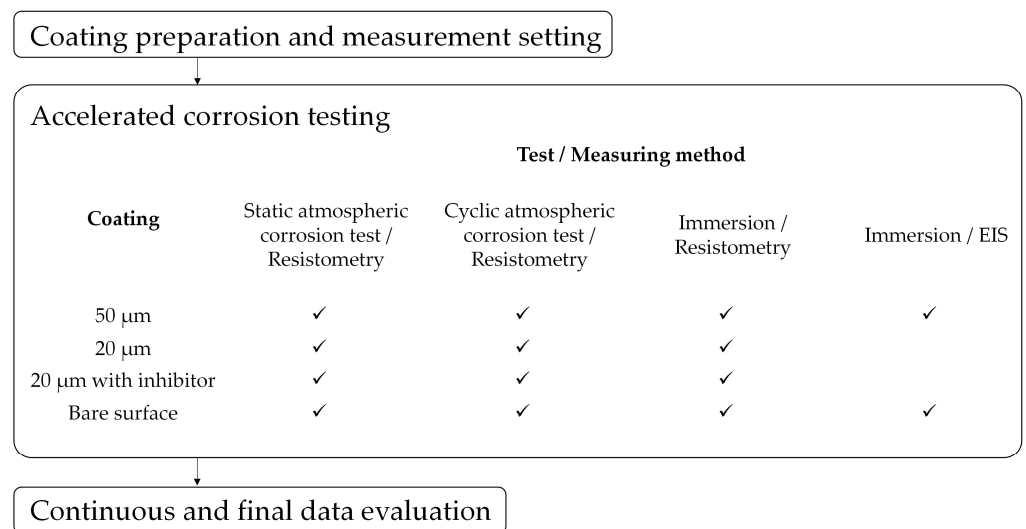


Figure 7. The experimental workflow.

### 3. Results

#### 3.1. Static Atmospheric Corrosion Test

The bare steel sensor, not protected by the coating, was activated on the first day of exposure when the humidity reached 93% RH after sealing the box. After the initial activation, the sensor corroded gradually throughout the exposure at a rate of  $39 \pm 12 \text{ nm} \cdot \text{day}^{-1}$  (average for the three sensing tracks).

The sensors protected by the  $50 \mu\text{m}$  coating and the  $20 \mu\text{m}$  coating with tannic acid detected no corrosion during the 2-month exposure, and no visible corrosion damage was observed on the measuring tracks.

Figure 8 shows the corrosion depth evolution for the sensor covered with the  $20 \mu\text{m}$  coating without inhibitor. The blue curve shows the RH, which gradually increased after sealing the box and stabilized at 100% RH after one week of exposure. Two of the three sensing tracks detected a thickness loss due to corrosion. Sensing track 3 was activated during the third day of exposure when the RH exceeded 94%, as indicated by the yellow arrow in the graph, and had been corroding gradually since then at approximately  $0.4 \text{ nm} \cdot \text{day}^{-1}$ . Sensing track 2 was activated on the seventh day of exposure after the RH exceeded 97%, as indicated by the grey arrow in the graph. In contrast to the gradually corroding track 3, two periods of rapid increase in the corrosion depth (i.e., higher corrosion rate) can be distinguished. They can be linked to the localization of corrosion, which inherently affects the electrical resistance measurement [4]. The corrosion rate reached a maximum of  $4.8 \text{ nm} \cdot \text{day}^{-1}$  between days 16 and 17. No activation was detected by sensing track 1. The difference between the three sensing tracks can be explained by the random distribution of defects inevitably present in any organic coating.

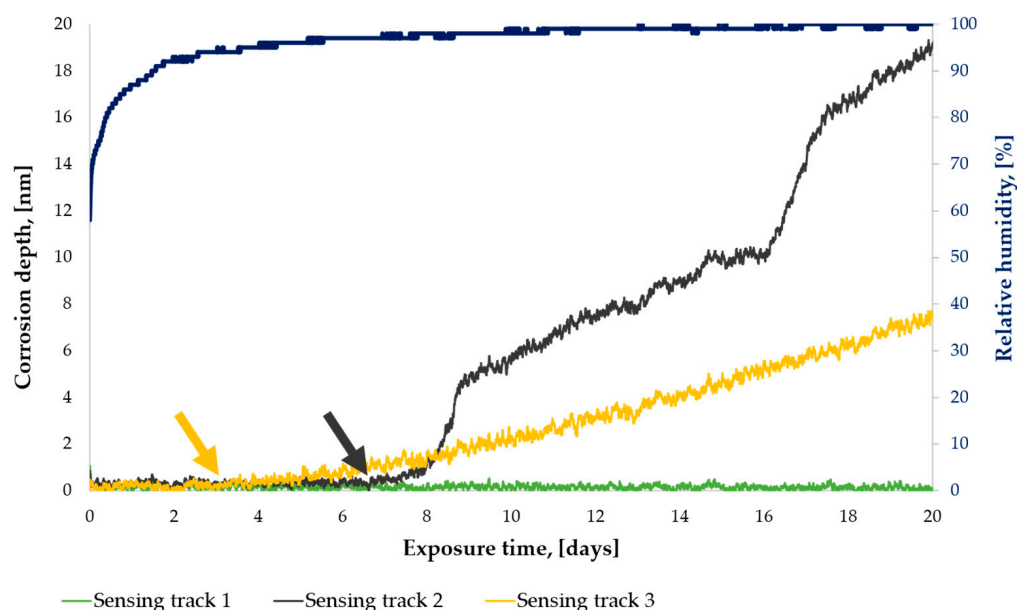


**Figure 8.** The corrosion depth measured on the sensor with the  $20 \mu\text{m}$  coating without an inhibitor during the first 20 days of the static atmospheric corrosion test; arrows indicate corrosion activation of sensing tracks 3 and 2.

#### 3.2. Cyclic Atmospheric Corrosion Test

Corrosion activation was detected by all sensors from the beginning of the exposure. Figure 9 shows the real-time corrosion rate measured by the coated sensors during the first four days. Since the corrosion rates recorded by the three tracks were always similar, average data are shown for better clarity. The RH record proves that the actual RH differed from that planned (see Figure 3). This was due to the slow kinetics of the humidity stabilization in the box after each opening. Nevertheless, the intended wet–dry cycling was achieved. All sensors detected cyclic increases and decreases in the corrosion rate

corresponding to the dynamic humidity changes. During the first two days of exposure, the corrosion rate was rather similar for the three sensors protected with different coating systems. A clear increase in the corrosion rate of the sensor with the 20  $\mu\text{m}$  coating without an inhibitor was observed during the third day of exposure, with the difference becoming even more significant during the fourth day, as indicated by the purple rectangles.

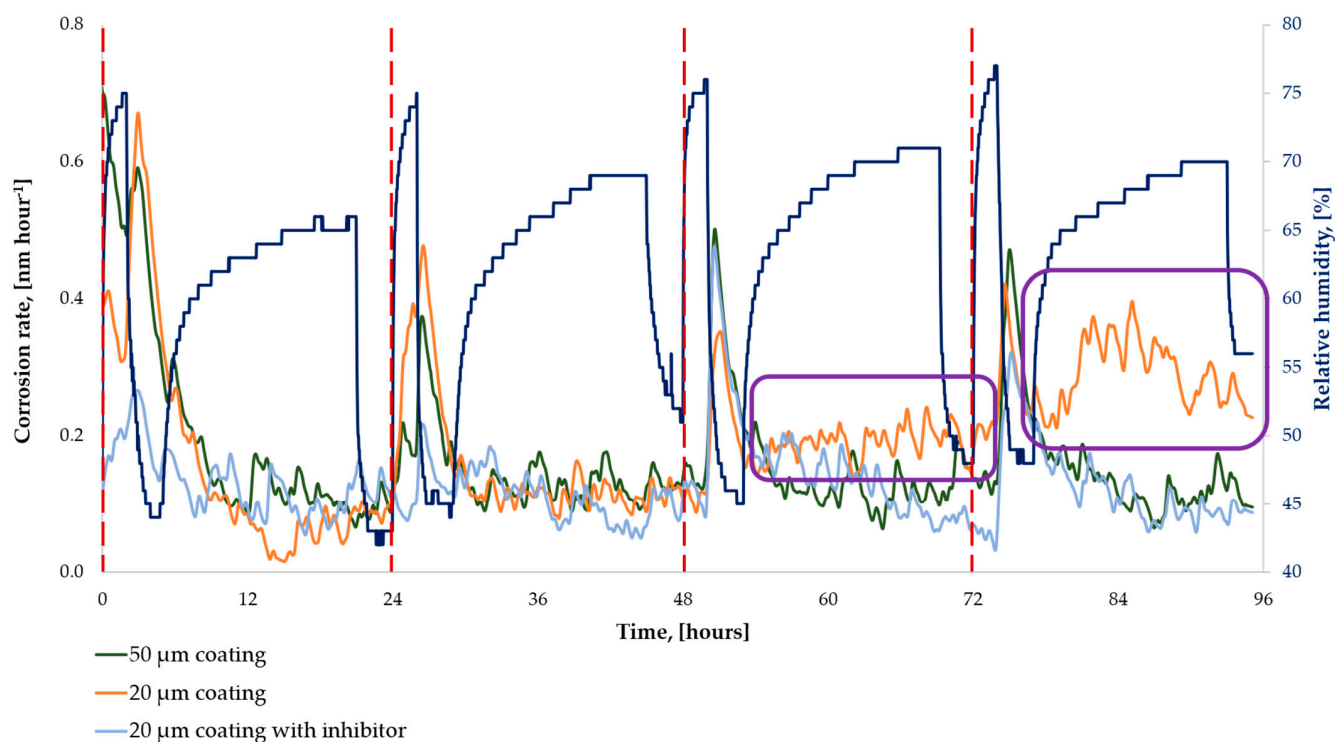


**Figure 9.** The corrosion rates of the coated sensors during the first 4 days of the cyclic atmospheric corrosion test: red dashed lines indicate the NaCl application; purple rectangles indicate an increase in the corrosion rate recorded by the sensor protected with the 20  $\mu\text{m}$  coating without an inhibitor during the wet phases on the third and fourth days of exposure.

Figure 10 shows a detail of the recorded data for the coated and bare sensors during the first 36 h of exposure. It illustrates the dynamics of the corrosion rate during particular test phases.

As shown in Figure 10a, all coated sensors were activated already by the first application of the chloride solution. The corrosion rate increased throughout the wet phase and then reached the maximum during the subsequent drying phase, when the humidity decreased to 50% RH. During the following wet and dry phases, the corrosion rate decreased and remained low until the next activation with chlorides. Similar dynamics can be observed for the bare sensor (Figure 10b), with a peak in the corrosion rate during the dry phase being particularly evident after the second NaCl deposition. The corrosion rates of the bare sensor were three orders of magnitude higher than those of the coated sensors, and the sensor completely corroded during the first week of exposure.

An additional experiment with sensors protected with 50  $\mu\text{m}$  coatings and sprayed with demineralized water and 0.3 and 1.5 wt.% NaCl that aimed to illustrate the effect of chloride concentration showed similar corrosion activation dynamics for the sensor sprayed with 1.5 wt.% NaCl. The maximum corrosion rate detected during the drying phase was 2  $\text{nm hour}^{-1}$ , which is 3 to 5 times higher than that of the same type of sensor sprayed with 0.3 wt.% NaCl. At the same time, no activation was detected during the drying of the sensor sprayed with demineralized water. Obviously, the chloride concentration played a key role in the observed coating degradation and steel substrate activation.

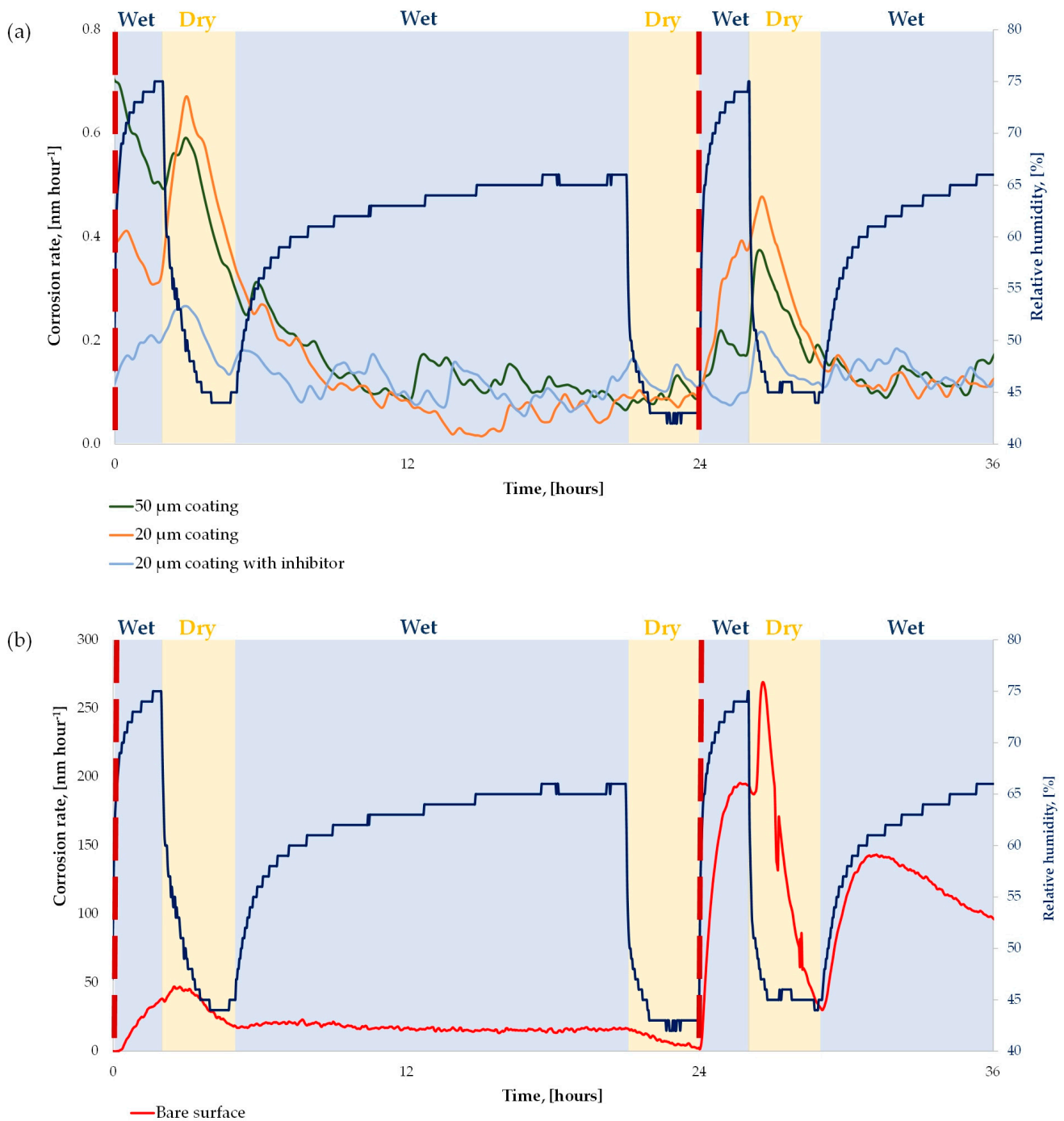


**Figure 10.** The real-time corrosion rates during the first 36 h of the cyclic atmospheric corrosion test: (a) coated sensors; (b) bare sensor; red dashed lines indicate the NaCl application.

### 3.3. Immersion Test

The bare sensor was activated immediately after immersion. It corroded gradually at  $841 \pm 85 \text{ nm} \cdot \text{day}^{-1}$ . The sensors protected with the 50 μm coating and the 20 μm coating with tannic acid detected no corrosion during two months of exposure.

The corrosion depth measurement and visual appearance of the sensor with the 20 μm coating without an inhibitor is shown in Figure 11. As shown in Figure 11a, the corrosion of all three sensing tracks activated after 2 days of immersion. Then, a further increase in the corrosion rate could be observed between days 18 and 23. It could be attributed to coating delamination caused by the formation of corrosion products under the coating. The sensor was significantly corroded after two months of immersion (Figure 11b). Both a dark and

rather uniform film and orange localized spots of corrosion products could be observed under the coating.

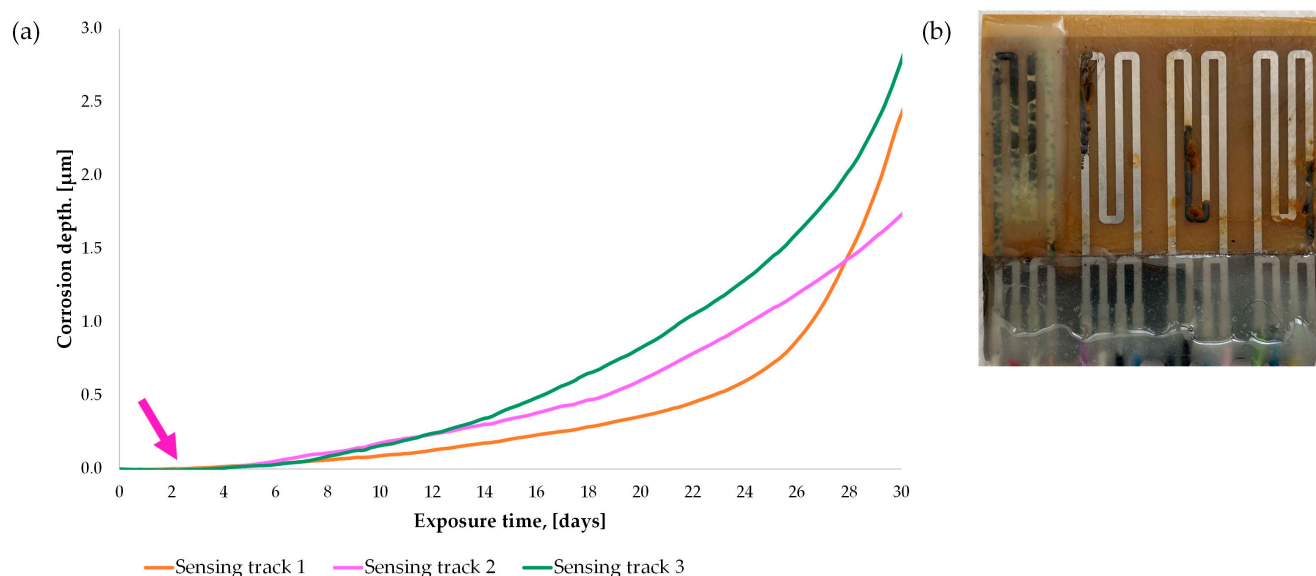


**Figure 11.** The sensor with the 20 µm coating without an inhibitor exposed in the immersion test: (a) the corrosion depth recorded during the first month of exposure; (b) the appearance of the sensor after two months of exposure; the arrow indicates the initial corrosion activation.

### 3.4. Comparison of Coating Performance

Table 1 summarizes the corrosion depth measured on the sensors after 2 weeks of exposure. The 2-week exposure was chosen for the comparison because some of the sensors completely corroded or stopped measuring correctly due to the insufficient protection of the reference track after this period. In the immersion and cyclic atmospheric test, the 20 µm coating was not sufficient to protect the metallic substrate. The same trend was observed in the static atmospheric test, although the activation occurred later and the results obtained from the three sensing tracks showed a large deviation. The application of the thicker coating or the inhibitor addition significantly improved the protective ability. For the bare metal, both static and cyclic atmospheric tests proved to be very corrosive, and the sensors corroded completely in less than 2 weeks. The corrosion rate in immersion was lower, probably due to limited oxygen access in the non-stirred bulk solution.

**Table 1.** Corrosion depths of resistometric sensors recorded after 2 weeks of exposure.

Exposure Conditions	Coating	Corrosion Depth [nm]
Static atmospheric test	50 µm	2 ± 1
	20 µm	2 ± 2
	20 µm + inhibitor	<DL
	Bare surface	>12,500 <sup>1</sup>
Immersion	50 µm	<DL
	20 µm	260 ± 66
	20 µm + inhibitor	<DL
	Bare surface	10,970 ± 1534
Cyclic atmospheric test	50 µm	<1
	20 µm	16 ± 1
	20 µm + inhibitor	<1
	Bare surface	>12,500 <sup>1</sup>

DL: Detection limit of the technique; <sup>1</sup> the sensor corroded in less than 2 weeks.

### 3.5. Electrochemical Impedance Spectroscopy

The graphs in Figures 12 and 13 represent the Bode plots of the impedance modulus  $Z$  and phase angle measured on the sensor with the 50  $\mu\text{m}$  coating and the bare sensor, respectively.

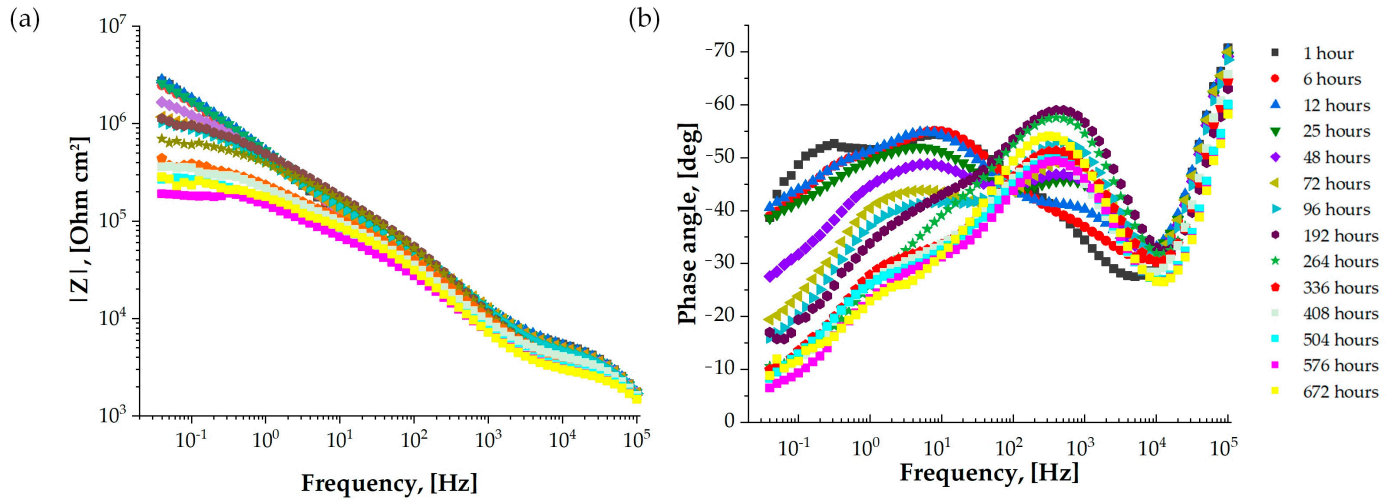


**Figure 12.** The EIS results (Bode plots) measured on the sensor with the 50  $\mu\text{m}$  coating: (a) impedance modulus; (b) phase angle.

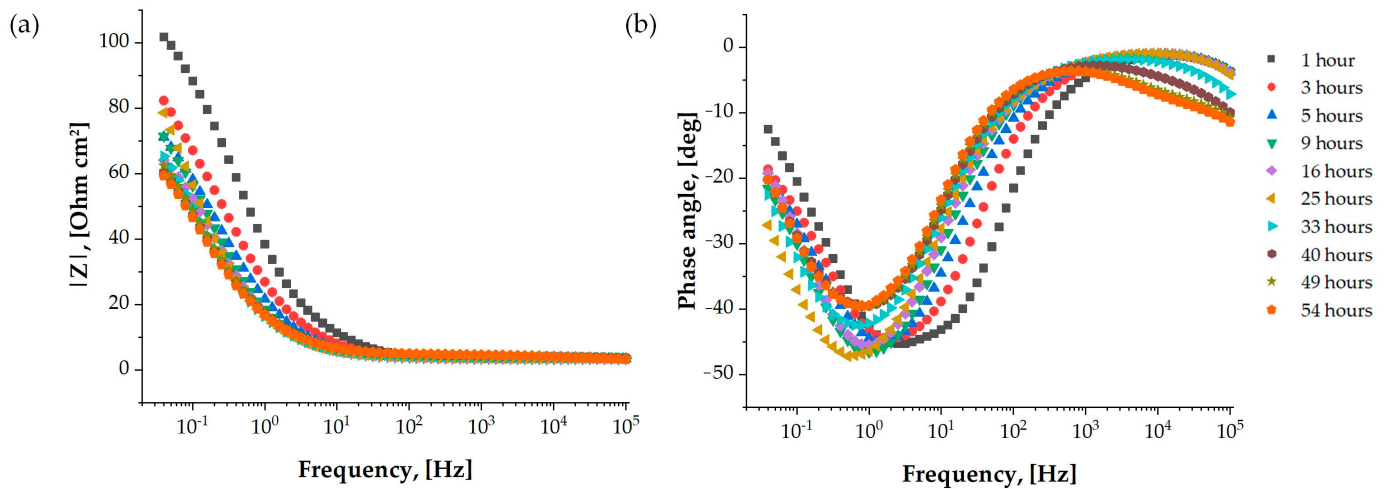


**Figure 13.** The EIS results (Bode plots) measured on the bare sensor: (a) impedance modulus; (b) phase angle.

The bare sensor showed a resistive plateau at high frequencies and a gradual decrease in overall impedance throughout the immersion period. The gradual accumulation of corrosion products over the sensor surface, as seen in the immersion test, reduced the exposed area and attenuated the impedance drop over time. The maximum impedance values  $|Z|$  recorded at low frequencies are below 100  $\text{Ohm cm}^2$ , indicating a quite high corrosion activity for the sensors, in good agreement with the previous results. The coated sensor showed a completely distinct behaviour. At high frequencies, a well-defined time constant was observed, as expected, evidencing the presence of the protective coating. With time, its resistance dropped slightly, but the phase angle remained quite stable, evidencing that the coating remained protective. At low frequencies, the overall impedance values were above 1  $\text{M}\Omega\text{cm}^2$  in the early stages, and these high impedance values, accounting for a well-protected surface, decayed slowly over the first week of immersion, revealing electrolyte uptake and activation of the bare metal. The more pronounced decay after

approximately one week accounts for the development of corrosion activity and its gradual process underneath the coating.

#### 4. Discussion

The results of both atmospheric and immersion tests show the high protective efficiency of the 50  $\mu\text{m}$  coating and the 20  $\mu\text{m}$  coating with the inhibitor, while the 20  $\mu\text{m}$  coating without the inhibitor proves to be insufficient to protect the steel substrate from corrosion. The high efficiency of the 50  $\mu\text{m}$  coating is consistent with the fact that the degree of protection depends on the coating thickness [3,29]. The improved protection of the thicker coating is linked to the formation of a thicker barrier between the metal surface and the corrosive environment, which prolongs the diffusion path for moisture, oxygen and corrosive ions. The high protective ability of the thinner coating with the inhibitor proves the previously reported efficiency of tannic acid in protecting steel by forming insoluble complexes with the metal substrate [9,60]. The corrosion of the reference track and electrical contacts, also reported by Zajec et al. in ref. [16], highlights the importance of proper coverage of these critical areas to achieve the corrosion protection greater than that of the tested coating.

Interesting results were obtained from the resistometric sensors exposed in the cyclic atmospheric test, where increases in the corrosion rate were repeatedly detected by all sensors during the drying phase after chloride deposition. Drying has previously been reported to be a particularly important process, leading to the acceleration of the atmospheric corrosion of bare steel and aluminium [44,45,56]. The following explanation for the effect of drying has been proposed [44,45,47,56]. When the RH is high, the metal surface is covered with a thick layer of electrolyte. The concentration of corrosive ions, particularly chlorides, in the dilute electrolyte is low, and the diffusion path for atmospheric oxygen through the thick layer is long, limiting its access to the metal surface. As the RH decreases, the water evaporates and the surface electrolyte layer becomes thinner, the chloride concentration increases and the access of atmospheric oxygen is facilitated. This creates highly corrosive conditions and accelerates corrosion. Then, as the drying continues, the electrolyte evaporates completely, resulting in the crystallization of chloride salts on the surface and low down or full inhibition of corrosion.

Considering the inevitable presence of coating defects, which allow the penetration of a water electrolyte, oxygen and corrosive ions to the metal substrate and induce the activation of corrosion [3,7,9,11], the corrosion rate evolution recorded by the resistometric sensors can be explained by the mechanism schematically illustrated in Figure 14. In humid atmosphere, a thick electrolyte layer forms on the surface and penetrates through defects to the metal surface (Figure 14a). During drying (Figure 14b), the electrolyte gradually evaporates from the coated surface, reducing the diffusion path for oxygen transport. Inside the defect, the evaporation is delayed, which results in the formation of a more concentrated electrolyte and corrosion acceleration. The key role of the presence of chloride ions at this stage is illustrated by the results of the verification test, which showed the accelerating effect of the increased concentration of the applied chloride solution, whereas no activation was detected by the sensor sprayed with demineralized water. As the drying continues, the electrolyte in the defect will eventually dry out, and the corrosion process will be interrupted (Figure 14c).

The EIS results showed that the bare sensor was activated at an early stage of immersion and the corrosion activity developed gradually, in agreement with the resistometric results. The presence of small defects and pores in the coating made EIS very sensitive to the early corrosion onset of the coated sensor during immersion. This effect was not as evident in the resistometric measurement, demonstrating the importance of combining different test methods to better characterize sensor health.

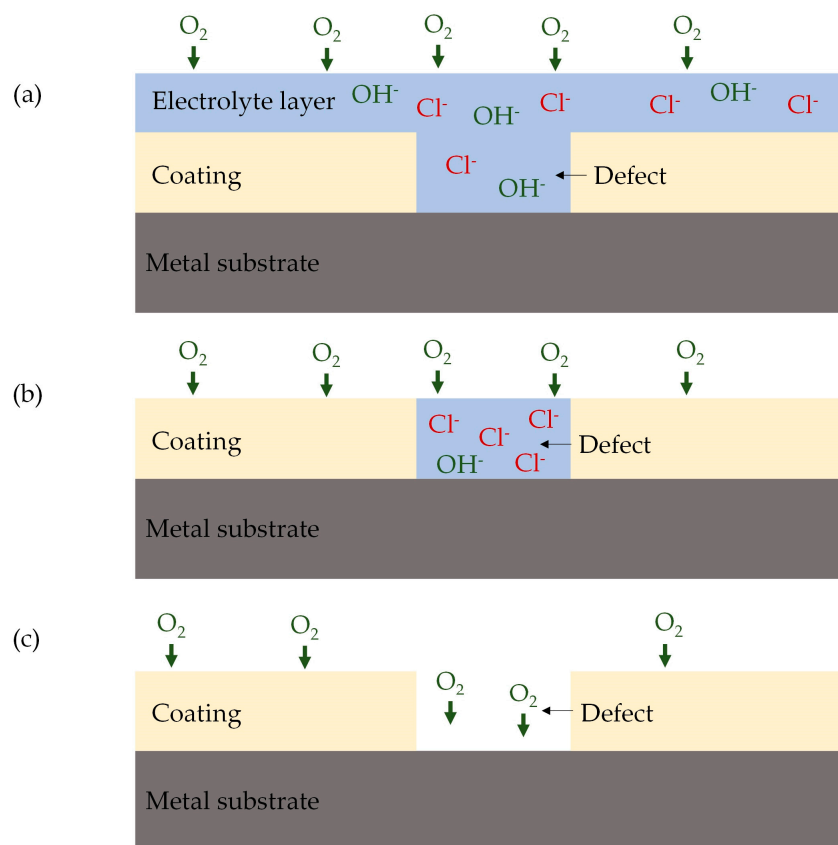


**Figure 14.** The mechanism of corrosion activation during the drying stage of the cyclic accelerated corrosion test: (a) wet phase; (b) drying process; (c) dry surface.

## 5. Conclusions

This study demonstrated the applicability of resistometric sensors for the evaluation of the protective effect of a polyolefin coating applied at two thicknesses with and without an inhibitor. The following conclusions can be drawn:

- Resistometric sensors have been shown to have a strong potential for the evaluation of the protective efficiency of organic coatings in both immersion and atmosphere. They provide particularly interesting information on the coating performance under dynamic atmospheric conditions, which better reflect typical operating conditions.
- The corrosion of the steel substrate increased strongly during drying. It can be explained by the shortening of the oxygen diffusion path and the formation of a highly concentrated electrolyte in coating defects.
- The protective ability of the coating increased with increasing thickness and the addition of the inhibitor.
- The potential limitations of using the resistometric technique lie mainly in the need for the efficient corrosion protection of the sensor reference track and electrical contacts.

The simple and straightforward operating principle and data interpretation, together with the ability to produce sensors of different thicknesses combining different substrates and coating systems, will allow for the future use of highly sensitive resistometric sensors for laboratory testing and thick robust sensors for long-term industrial applications.

**Author Contributions:** Conceptualization, K.P. and M.F.M.; methodology, K.P., M.F.M. and T.P.; validation, M.F.M. and T.P.; formal analysis, K.P., M.F.M. and T.P.; investigation, K.P.; resources, K.P., M.F.M. and T.P.; data curation, K.P. and M.F.M.; writing—original draft preparation, K.P.; writing—review and editing, M.F.M. and T.P.; visualization, K.P., M.F.M. and T.P.; supervision, M.F.M. and T.P.; project administration, M.F.M. and T.P.; funding acquisition, T.P. All authors have read and agreed to the published version of the manuscript.

**Funding:** This research was partly funded by the Technological Agency of the Czech Republic (TAČR), grant number FW01010482. The laboratory work was carried out during the traineeship within the Erasmus+ mobility programme.

**Data Availability Statement:** The data presented in this study are available on request from the corresponding author.

**Acknowledgments:** The authors thank Tiago Silva for his help with the coating preparation and EIS measurements. M. F. Montemor thanks the CQE Research Unit funded by FCT through projects <https://doi.org/10.54499/UIBP/00100/2020> (accessed on 14 November 2024) and <https://doi.org/10.54499/UIBP/00100/2020> (accessed on 14 November 2024). We also thank the Institute of Molecular Sciences Associate Laboratory funded by FCT through project <https://doi.org/10.54499/LA/P/0056/2020> (accessed on 14 November 2024).

**Conflicts of Interest:** The authors declare no conflicts of interest.

## References

1. Koch, G. Cost of corrosion. In *Trends in Oil and Gas Corrosion Research and Technologies*; Woodhead Publishing: Amsterdam, The Netherlands, 2017; pp. 3–30. [CrossRef]
2. Silva, T.A.R.; Marques, A.C.; dos Santos, R.G.; Shakoor, R.A.; Taryba, M.; Montemor, M.F. Development of BioPolyurethane Coatings from Biomass-Derived Alkylphenol Polyols—A Green Alternative. *Polymers* **2023**, *15*, 2561. [CrossRef] [PubMed]
3. Sorensen, P.A.; Kiil, S.; Dam-Johansen, K.; Weinell, C.E. Anticorrosive coatings: A review. *J. Coat. Technol. Res.* **2009**, *6*, 135–176. [CrossRef]
4. Popova, K.; Prošek, T. Corrosion Monitoring in Atmospheric Conditions: A Review. *Metals* **2022**, *12*, 171. [CrossRef]
5. Bender, R.; Féron, D.; Mills, D.; Ritter, S.; Bäßler, R.; Bettge, D.; De Graeve, I.; Dugstad, A.; Grassini, S.; Hack, T.; et al. Corrosion challenges towards a sustainable society. *Mater. Corros.* **2022**, *73*, 1730–1751. [CrossRef]
6. Talbot, D.E.J.; Talbot, J.D.R. *Corrosion Science and Technology*, 3rd ed.; Taylor & Francis: Boca Raton, FL, USA, 2018; pp. 1–568.
7. Montemor, M.F. Functional and smart coatings for corrosion protection: A review of recent advances. *Surf. Coat. Technol.* **2014**, *258*, 17–37. [CrossRef]
8. Cui, G.; Bi, Z.; Wang, S.; Liu, J.; Xing, X.; Li, Z.; Wang, B. A comprehensive review on smart anti-corrosive coatings. *Prog. Org. Coat.* **2020**, *148*, 105821. [CrossRef]
9. Raj, R.; Kahraman, R.; Shakoor, A.; Montemor, M.F.; Taryba, M. Tannic Acid-Loaded Hydroxyapatite Carriers for Corrosion Protection of Polyolefin-Coated Carbon Steel. *Appl. Sci.* **2022**, *12*, 10263. [CrossRef]
10. Raj, R.; Taryba, M.; Morozov, Y.; Kahraman, R.; Shakoor, R.A.; Montemor, M.F. On the synergistic corrosion inhibition and polymer healing effects of polyolefin coatings modified with Ce-loaded hydroxyapatite particles applied on steel. *Electrochim. Acta* **2021**, *388*, 138648. [CrossRef]
11. Trentin, A.; Pakseresht, A.; Duran, A.; Castro, Y.; Galusek, D. Electrochemical Characterization of Polymeric Coatings for Corrosion Protection: A Review of Advances and Perspectives. *Polymers* **2022**, *14*, 2306. [CrossRef]
12. Calado, L.M.; Taryba, M.; Morozov, Y.; Carmezim, M.J.; Montemor, M.F. Novel smart and self-healing cerium phosphate-based corrosion inhibitor for AZ31 magnesium alloy. *Corros. Sci.* **2020**, *170*, 108648. [CrossRef]
13. *ISO 12944-2:2017*; Paints and Varnishes—Corrosion Protection of Steel Structures by Protective Paint Systems—Part 2: Classification of Environments. ISO: Genève, Switzerland, 2017.
14. Zajec, B.; Bajt Leban, M.; Kosec, T.; Kuhar, V.; Legat, A.; Lenart, S.; Fifer Bizjak, K.; Gavin, K. Corrosion Monitoring of Steel Structure Coating Degradation. *Teh. Vjesn.* **2018**, *25*, 1348–1355. [CrossRef]
15. Hoseinpoor, M.; Prošek, T.; Babusiaux, L.; Mallegol, J. Toward more realistic time of wetness measurement by means of surface relative humidity. *Corros. Sci.* **2020**, *177*, 108999. [CrossRef]
16. Zajec, B.; Leban, M.B.; Lenart, S.; Gavin, K.; Legat, A. Electrochemical impedance and electrical resistance sensors for the evaluation of anticorrosive coating degradation. *Corros. Rev.* **2017**, *35*, 65–74. [CrossRef]
17. Deng, F.; Huang, Y.; Azarmi, F. Corrosion Behavior Evaluation of Coated Steel Using Fiber Bragg Grating Sensors. *Coatings* **2019**, *9*, 55. [CrossRef]
18. *ISO 12944-6:2018*; Paints and Varnishes—Corrosion Protection of Steel Structures by Protective Paint Systems—Part 6: Laboratory Performance Test Methods. ISO: Genève, Switzerland, 2018.
19. *ISO 4628:2016*; Paints and Varnishes—Evaluation of Degradation of Coatings—Designation of Quantity and Size of Defects, and of Intensity of Uniform Changes in Appearance. ISO: Genève, Switzerland, 2016.
20. Upadhyay, V.; Battocchi, D. Localized electrochemical characterization of organic coatings: A brief review. *Prog. Org. Coat.* **2016**, *99*, 365–377. [CrossRef]
21. Habib, S.; Nawaz, M.; Kahraman, R.; Ahmed, E.M.; Shakoor, R.A. Effect of the modified hybrid particle on the corrosion inhibition performance of polyolefin based coatings for carbon steel. *J. Sci.-Adv. Mater. Dev.* **2022**, *7*, 100466. [CrossRef]
22. Nazarov, A.; Prošek, T.; Thierry, D. Application of EIS and SKP methods for the study of the zinc/polymer interface. *Electrochim. Acta* **2008**, *53*, 7531–7538. [CrossRef]

23. Cano, E.; Lafuente, D.; Bastidas, D.M. Use of EIS for the evaluation of the protective properties of coatings for metallic cultural heritage: A review. *J. Solid State Electr.* **2010**, *14*, 381–391. [[CrossRef](#)]
24. Loveday, D.; Peterson, P.; Rodgers, B. Evaluation of organic coatings with electrochemical impedance spectroscopy—Part 1: Fundamentals of electrochemical impedance spectroscopy. *JCT J. Coat. Technol.* **2004**, *1*, 46–52.
25. Rammelt, U.; Reinhard, G. Application of Electrochemical Impedance Spectroscopy (EIS) for Characterizing the Corrosion-Protective Performance of Organic Coatings on Metals. *Prog. Org. Coat.* **1992**, *21*, 205–226. [[CrossRef](#)]
26. Amirudin, A.; Thierry, D. Application of electrochemical impedance spectroscopy to study the degradation of polymer-coated metals. *Prog. Org. Coat.* **1995**, *26*, 1–28. [[CrossRef](#)]
27. Margarit-Mattos, I.C.P. EIS and organic coatings performance: Revisiting some key points. *Electrochim. Acta* **2020**, *354*, 136725. [[CrossRef](#)]
28. Xia, D.H.; Deng, C.-M.; Macdonald, D.; Jamali, S.; Mills, D.; Luo, J.-L.; Strebl, M.G.; Amiri, M.; Jin, W.; Song, S.; et al. Electrochemical measurements used for assessment of corrosion and protection of metallic materials in the field: A critical review. *J. Mater. Sci. Technol.* **2022**, *112*, 151–181. [[CrossRef](#)]
29. Diler, E.; Ledan, F.; LeBozec, N.; Thierry, D. Real-time monitoring of the degradation of metallic and organic coatings using electrical resistance sensors. *Mater. Corros.* **2017**, *68*, 1365–1376. [[CrossRef](#)]
30. Mansfeld, F. Use of Electrochemical Impedance Spectroscopy for the Study of Corrosion Protection by Polymer Coatings. *J. Appl. Electrochem.* **1995**, *25*, 187–202. [[CrossRef](#)]
31. Alamin, M.; Tian, G.Y.; Andrews, A.; Jackson, P. Corrosion detection using low-frequency RFID technology. *Insight* **2012**, *54*, 72–75. [[CrossRef](#)]
32. Alamin, M. Passive Low Frequency RFID for Detection and Monitoring of Corrosion Under Paint and Insulation. Ph.D. Thesis, Newcastle University, Newcastle upon Tyne, UK, 2014.
33. Sunny, A.I.; Tian, G.Y.; Zhang, J.; Pal, M. Low frequency (LF) RFID sensors and selective transient feature extraction for corrosion characterisation. *Sens. Actuators A Phys.* **2016**, *241*, 34–43. [[CrossRef](#)]
34. Daneshian, B.; Höche, D.; Knudsen, O.Ø.; Skilbred, A.W.B. Effect of climatic parameters on marine atmospheric corrosion: Correlation analysis of on-site sensors data. *npj Mat. Degrad.* **2023**, *7*, 10. [[CrossRef](#)]
35. Seghier, M.E.A.B.; Knudsen, O.Ø.; Skilbred, A.W.B.; Höche, D. An intelligent framework for forecasting and investigating corrosion in marine conditions using time sensor data. *npj Mat. Degrad.* **2023**, *7*, 91. [[CrossRef](#)]
36. Tatsuoaka. Under-film Corrosion Monitoring by Painted Electrodes in High Humid Environment. In Proceedings of the EU-ROCORR 2024, Paris, France, 1–5 September 2024.
37. Švadlena, J.; Stouřil, J. Evaluation of protective properties of acrylate varnishes used for conservation of historical metal artefacts. *KOM—Corros. Mater. Prot. J.* **2017**, *61*, 25–31. [[CrossRef](#)]
38. Švadlena, J.; Voracova, E.; Stouřil, J. Corrosion of silver in environment containing halides, pseudohalides, or thiourea. *Mater. Corros.* **2020**, *71*, 1721–1728. [[CrossRef](#)]
39. Prošek, T.; Taube, M.; Dubois, F.; Thierry, D. Application of automated electrical resistance sensors for measurement of corrosion rate of copper, bronze and iron in model indoor atmospheres containing short-chain volatile carboxylic acids. *Corros. Sci.* **2014**, *87*, 376–382. [[CrossRef](#)]
40. Prošek, T.; Dubois, F.; Kouřil, M.; Scheffel, B.; Degres, Y.; Jouannic, M.; Taube, M.; Dubus, M.; Hubert, V.; Thierry, D. Application of automated corrosion sensors for real-time monitoring in atmospheres polluted with organic acids. In Proceedings of the 18th International Corrosion Congress 2011, Perth, WA, Australia, 20–24 November 2011.
41. Msallamová, Š.; Kouřil, M.; Strachotová, K.C.; Stouřil, J.; Popova, K.; Dvořáková, P.; Lhotka, M. Protection of lead in an environment containing acetic acid vapour by using adsorbents and their characterization. *Herit. Sci.* **2019**, *7*, 76. [[CrossRef](#)]
42. Msallamová, Š.; Kouřil, M.; Strachotová, K.C.; Stouřil, J.; Popova, K.; Dvořáková, P. Historical lead seals and the influence of disinfectants on the lead corrosion rate. *Herit. Sci.* **2019**, *7*, 18. [[CrossRef](#)]
43. Strachotová, K.C.; Kuchťáková, K.; Kouřil, M.; Msallamová, Š. Protection of Lead in Acetic Acid Containing Air by Means of Corrosion Inhibitors. In Proceedings of the 27th International Conference on Metallurgy and Materials (Metal 2018), Brno, Czech Republic, 23–25 May 2018; pp. 1045–1050.
44. Prošek, T.; Le Bozec, N.; Thierry, D. Application of automated corrosion sensors for monitoring the rate of corrosion during accelerated corrosion tests. *Mater. Corros.* **2014**, *65*, 448–456. [[CrossRef](#)]
45. Diler, E.; Peltier, F.; Becker, J.; Thierry, D. Real-time corrosion monitoring of aluminium alloys under chloride-contaminated atmospheric conditions. *Mater. Corros.* **2021**, *72*, 1377–1387. [[CrossRef](#)]
46. Gao, G.; Wang, T.; Makeyev, V. Corrosion Rates of Steel, Zinc and Bi-Metal Couples in the Field and in Laboratory Environments. *SAE Trans.* **2002**, *111*, 355–373.
47. Van den Steen, N.; Simillion, H.; Thierry, D.; Deconinck, J. Modeling Film Thicknesses and Estimating Corrosion Depths Under Climate Control. In *ECS Meeting Abstracts*; IOP Publishing: Bristol, UK, 2016.
48. Van den Steen, N.; Simillion, H.; Thierry, D.; Deconinck, J. Comparing Modeled and Experimental Accelerated Corrosion Tests on Steel. *J. Electrochem. Soc.* **2017**, *164*, C554–C562. [[CrossRef](#)]
49. Dubus, M.; Prošek, T. Standardized assessment of cultural heritage environments by electrical resistance measurements. *E-Preserv. Sci.* **2012**, *9*, 67–71.

50. Kouřil, M.; Prošek, T.; Dubus, M.; Taube, M.; Hubert, V.; Scheffel, B.; Degres, Y.; Jouannic, M.; Thierry, D. Korozní monitoring v rukách restaurátorů a konzervátorů/Corrosion monitoring in the hands of restorers and conservators. *KOM–Corros. Mater. Prot. J.* **2012**, *56*, 67–75.
51. Prošek, T.; Kouřil, M.; Dubus, M.; Taube, M.; Hubert, V.; Scheffel, B.; Degres, Y.; Jouannic, M.; Thierry, D. Real-time monitoring of indoor air corrosivity in cultural heritage institutions with metallic electrical resistance sensors. *Stud. Conserv.* **2013**, *58*, 117–128. [[CrossRef](#)]
52. Kreislová, K.; Fialová, P.; Boháčková, T. Indoor corrosivity in Klementinum baroque library hall, Prague. *WIT Trans. Built Environ.* **2021**, *203*, 123–131.
53. Kouřil, M.; Prošek, T.; Scheffel, B.; Degres, Y. Corrosion monitoring in archives by the electrical resistance technique. *J. Cult. Herit.* **2014**, *15*, 99–103. [[CrossRef](#)]
54. Vaissière, L.; Ragazzini, M.; Despert, G.; LeBozec, N.; Thierry, D. Cartography of corrosion aggressivity on vehicle in dynamic corrosion test in Renault. In Proceedings of the EUROCORR, Stockholm, Sweden, 4–8 September 2011; pp. 4–8.
55. Kosec, T.; Kuhar, V.; Kranjc, A.; Malnaric, V.; Belingar, B.; Legat, A. Development of an Electrical Resistance Sensor from High Strength Steel for Automotive Applications. *Sensors* **2019**, *19*, 1956. [[CrossRef](#)]
56. Popova, K.; Prošek, T.; Šefl, V.; Šedivý, M.; Kouřil, M.; Reiser, M. Application of flexible resistometric sensors for real-time corrosion monitoring under insulation. *Mater. Corros.* **2024**, *75*, 625–635. [[CrossRef](#)]
57. Li, Z.L.; Fu, D.M.; Li, Y.; Wang, G.Y.; Meng, J.T.; Zhang, D.W.; Yang, Z.H.; Ding, G.Q.; Zhao, J.B. Application of An Electrical Resistance Sensor-Based Automated Corrosion Monitor in the Study of Atmospheric Corrosion. *Materials* **2019**, *12*, 1065. [[CrossRef](#)]
58. Nawaz, M.; Kahraman, R.; Taryba, M.; Hassan, M.K.; Attaei, M.; Montemor, M.F.; Shakoore, R.A. Improved properties of polyolefin nanocomposite coatings modified with ceria nanoparticles loaded with 2-mercaptobenzothiazole. *Prog. Org. Coat.* **2022**, *171*, 107046. [[CrossRef](#)]
59. Attaei, M.; Taryba, M.; Shakoore, R.A.; Kahraman, R.; Marques, A.C.; Montemor, M.F. Highly protective polyolefin coating modified with ceria nano particles treated with N,N,N',N'-Tetrakis(2-hydroxyethyl)ethylenediamine for corrosion protection of carbon steel. *Corros. Sci.* **2022**, *198*, 110162. [[CrossRef](#)]
60. Both, J.; Szabó, G.S.; Katona, G.; Muresan, L.M. Anticorrosive polystyrene coatings modified with tannic acid on zinc and steel substrates. *J. Electrochem. Sci. Eng.* **2022**, *12*, 721–730. [[CrossRef](#)]
61. Van den Steen, N.; Simillion, H.; Dolgikh, O.; Terryn, H.; Deconinck, J. An integrated modeling approach for atmospheric corrosion in presence of a varying electrolyte film. *Electrochim. Acta* **2016**, *187*, 714–723. [[CrossRef](#)]

**Disclaimer/Publisher's Note:** The statements, opinions and data contained in all publications are solely those of the individual author(s) and contributor(s) and not of MDPI and/or the editor(s). MDPI and/or the editor(s) disclaim responsibility for any injury to people or property resulting from any ideas, methods, instructions or products referred to in the content.